Research Square

Preprints are preliminary reports that have not undergone peer review.
They should not be considered conclusive, used to inform clinical practice,
or referenced by the media as validated information.

A study of particle behaviour in dynamic extracellular environments using nanoparticles as model nanoscale probes

Genevieve Schleyer

G.Schleyer@liverpool.ac.uk

University of Liverpool

Eann A. Patterson

University of Liverpool

Judith M. Curran

University of Liverpool

Article

Keywords: nanoscale, diffusion, transport, extracellular, label free, microscopy

Posted Date: October 30th, 2026

DOI: https://doi.org/10.21203/rs.3.rs-11094060/v1

License: This work is licensed under a Creative Commons Attribution 4.0 International License.
Read Full License

Additional Declarations: No competing interests reported.

A study of particle behaviour in dynamic extracellular environments using nanoparticles as model nanoscale probes

Genevieve Schleyer*[1], Eann A. Patterson[2] and Judith M. Curran[1]

[1]Department of Materials, Design & Manufacturing Engineering, University of Liverpool, Brownlow Hill, Liverpool, UK

[2]Department of Mechanical and Aerospace Engineering, University of Liverpool, Brownlow Hill, Liverpool, UK

Key words: nanoscale, diffusion, transport, extracellular, label free, microscopy

Corresponding author: G.Schleyer@liverpool.ac.uk

Abstract

Quantifying nanoparticle behaviour in complex biological environments is essential for understanding transport and interactions within heterogeneous living systems. Fluorescent labelling is commonly used to visualise nanoparticles; however, surface modification by fluorescent probes can alter nanoparticle interactions and obscure native behaviour. Therefore, accessible label-free methods are needed to characterise nanoparticle dynamics under biologically relevant conditions. In this study, an optical caustics-based microscopy technique was used to track the motion of 100 nm gold nanoparticles in the extracellular space above human mesenchymal stem cell (hMSC) monolayers. Nanoparticle trajectories were analysed using diffusion coefficients, anomalous diffusion exponents, and convex hull metrics to quantify transport behaviour. Results demonstrated that the local extracellular environment significantly influences nanoparticle dynamics. In the presence of fetal bovine serum, nanoparticle diffusion rates changed significantly after one hour of exposure to the hMSC layer. Surface charge, protein content, and particle localisation relative to cells also had a marked effect on mobility. Comparison with idealised Brownian transport predictions showed that the living extracellular environment behaves as a dynamic and evolving transport medium that modifies nanoparticle movement. These findings highlight the sensitivity of nanoscale transport to local biological conditions and establish a label-free framework for investigating nanoparticle dynamics in heterogeneous biological systems.

Introduction

Understanding the transport of nanoscale entities in complex biological environments is a fundamental problem and various approaches have been taken to simulate stochastic motion in complex, heterogeneous or crowded environments [1]. Biological environments *in vitro* are dynamic as are the interactions that occur within them. In ideal fluids, particle transport can often be described by Brownian diffusion, where random thermal fluctuations produce diffusion and sedimentation that can be modelled with relatively simple relationships. In biological solutions and environments, however, the local surrounding environment of naturally occurring or introduced nanoscale entities is spatially heterogeneous and changes over time making it a dynamic environment. Physiological environments are host to many biological solutions, the components of which interact with nanoscale entities and potentially affect their dynamic behaviour. Diffusion plays a central role in nano entity transport and changes in mobility can influence both transport through biological matrices and opportunities for interaction with cellular interfaces [2]. In addition, cellular activity can lead to evolving microenvironment as proteins and extracellular matrix material is produced. Understanding how biological environments influence nanoscale transport therefore represents an important challenge in biophysics.

Biological transport processes occur across various systems and a large range of length scales including motion of proteins, extracellular vesicles, viral particles and bacteria. Calibrated nanoparticles provide a useful experimental model and tool for studying transport in complex biological media as their physicochemical properties can be finely tuned. Some studies have previously shown the importance of diffusion and particle mobility on the potential for future interaction with cellular surfaces and navigation through crowded environments [3-7] however more research is needed to fully understand the influence of biological interactions on nanoscale entity transport. Few studies have directly quantified nanoparticle dynamics during the approach to a cell surface.

Quantifying particle diffusion in biologically relevant environments remains a significant challenge, as nanoscale objects lie below the diffraction limit of visible light [8]. While their positions can be localized using single-molecule and single-particle tracking techniques these approaches typically rely on fluorescent labelling or specialized label-free detection methods. Fluorescence-based techniques including those employing quantum dots offer high sensitivity and spatial resolution [9]; however, the attachment of fluorophores can potentially affect particle–cell interactions through the modification of their surfaces or leaching of the

fluorescent dye into the system under study [10-12]. These perturbations, although subtle, would be particularly problematic in complex biological environments, where subtle physicochemical changes can potentially affect transport behaviour.

Label free approaches such as those based on interferometry [13,14], scattered light imaging [11], surface plasmon resonance microscopy (SPRM) [15], and photothermal imaging [16] overcome these limitations. However, many of these techniques require highly specialized instrumentation, limiting their accessibility and widespread application. As a result, there remains a clear need for low-cost, label-free methods that enable real-time, quantitative tracking of nanoparticles in complex biological environments without perturbing their native behaviour. Techniques such as reflection enhanced dark field scattering microscopy show promise due to their ease of application for tracking biological and metallic nanoparticles [17,18], but further development is required to achieve robust, widely applicable solutions for biophysical research.

In this study, we apply an optical caustics-based imaging approach to quantify nanoparticle transport in the extracellular space above living cell monolayers. This highly accessible, label free technique enables real time tracking of individual nanoparticles in complex *in vitro* environments, providing direct insight into how the presence of living cells modifies nanoparticle transport as a function of time, particle surface charge and surrounding protein environment. The method exploits the optical phenomenon of caustics [19] and has previously been validated for quantifying nanoparticle dynamics in simple solutions [20] and for characterising the dynamics of *Escherichia coli* [10].

The present work has used nanoparticles as proxies for a range of nanoscale entities to determine how heterogeneous, dynamic extracellular environments modify transport behaviour of nanoscale particles. We have tested whether living cell populations alter local transport conditions sufficiently to produce measurable changes in nanoparticle mobility and trajectory statistics. The results provide experimental evidence that cellular environments behave as dynamically evolving transport media whose influence extends beyond direct particle-cell contact and affects stochastic motion throughout the surrounding extracellular space.

Method and Materials

Human Mesenchymal Stem Cells (hMSCs)

Human mesenchymal stem cells (Lonza, UK; cat. no. PT-2501) at passage 4-6 were cultured at a seeding density of 10,000 cells/cm^2 on glass cover slips (Camlab, Academy, Over, UK; cat. no.

13/2222). The cover slips were kept in 6-well plates, each well containing one cover slip. The growth media consisted of Dulbecco's Modified Eagle medium (Fisher Scientific, Loughborough, Leicestershire, UK; cat. no. p-4919836), 10% Fetal Bovine Serum (Fisher Scientific, Loughborough, Leicestershire, UK, cat. no. 16629525), 1.2% L-Glutamine (Fisher Scientific, Loughborough, Leicestershire, UK; cat. no. 11534546), 1% Antibiotic-Antimycotic (Fisher Scientific, Loughborough, Leicestershire, UK; cat. no. 15963194) and 72µg L-Ascorbic acid 2-Phosphate sesquimagnesium salt hydrate (Sigma Aldrich, Saint Louis, MO, USA; cat. no. A8960). After seeding, cells were incubated at 37°C with 5% CO_2 and monitored for 96 hours, after which they were 90-95% confluent. The viability of cells was ascertained using trypan blue before seeding and using a LIVE/DEAD viability kit (Fisher Scientific, Loughborough, Leicestershire, UK; cat. no. L3224) after nanoparticle exposure. Cells were seeded with a viability of over 80%. Nanoparticle solutions were exposed to hMSCs on glass coverslips and incubated for two hours at 37°C and 5% CO_2 and the viability of the adherent monolayer evaluated using a live-dead immunofluorescent assay (Fisher Scientific, Loughborough, Leicestershire, UK; cat. no. L3224).

Nanoparticle solution

Negatively charged gold citrate nanoparticles were purchased in deionised water with a diameter of 100nm and zeta potential of ~-40mV as reported by the manufacturer (BBI Solutions, Crumlin, UK; cat. no. EM.GC100/7). Positively charged gold nanoparticles with branched polyethylenimine (BPEI) surfaces were purchased also with a diameter of 100nm and zeta potential of +59.4 mV (Nanocomposix, San Diego, CA, USA; cat. no. AUBB100-1M). Additionally, gold negatively charged (citrate) nanoparticles with a diameter of 50nm were purchased in deionised water (BBI Solutions, Crumlin, UK). Nanoparticles were dispersed in solutions of filtered Dulbecco's Modified Eagle Medium supplemented with 10% fetal bovine serum and Dulbecco's Modified Eagle Medium with no serum supplementation at a concentration of 10^7 particle/ml. The tracking media containing serum proteins was filtered using a 0.2µm syringe filter to remove large clumps of proteins to reduce background noise produced by caustic signatures. Nanoparticles in DMEM with 10% FBS were exposed to the tracking medium containing serum proteins for a maximum of 10 minutes before being placed in contact with the cell layer, at which point it was assumed they had already formed a protein corona consisting of serum proteins. To ensure monodispersion of the nanoparticle solutions and separate loosely aggregated particles, samples of nanoparticles in DMEM with and without FBS were first mixed to combine the nanoparticles with the media using a vortex mixer (Thermo Fisher) and then placed in a sonication bath for 5 minutes. Caustic signatures of single particles

can be easily distinguished from those of aggregated particles at the concentrations used in this study by their shape as demonstrated in our previous study [21]. 50 µl of the nanoparticle solution was placed in a 150 µm deep microscope slide cavity (Eisco, Victor, NY, USA, cat. no. BI0086B). Using tweezers, cover slips coated with hMSCs were removed from the wells and placed quickly but gently cell-side-down onto the microscope slide containing the nanoparticle solution. The edges of the cover slip were sealed with clear nail polish prior to tracking analysis.

Nanoparticle tracking

The samples were visualised in a standard inverted optical microscope (Axio Observer Z1, Carl Zeiss, Oberkochen, Germany) equipped with a condenser lens assembly and 40x magnification objective lens. To generate the caustic signatures of nanoparticles the adjustable condenser aperture was reduced to approximately 1 mm, and a narrow band (550 nm) filter was placed in the light path to increase the coherence of the light source which was a 100W halogen lamp. The microscope was set up for Kohler illumination to also increase the caustic imaging capability of the microscope [22]. The microscope was equipped with an incubation stage (Incubator PM S1, Temp and CO_2 module S1, Carl Zeiss, Oberkochen, Germany) which was set at 37 °C. A camera supported by the ZEN software (Axiocam z1.m, Carl Zeiss, Oberkochen, Germany) was used to visualise and record videos of the nanoparticles. The videos of the nanoparticles were recorded for a period of 2 seconds at 50 fps. The position of a nanoparticle can be determined by finding the brightest section of the three-dimensional optical signature which is demonstrated in figure 1. This appears as a bright spot surrounded with a dark ring (Figure 2) as explained by Patterson and Whelan [23]. As the objective plane is moved further away from the cells on the cover slip, their caustic signatures become out of focus, allowing the caustic signatures of nanoparticles to be seen (Figure 3).

Nanoparticles were tracked within discrete axial ranges above the cell layer to assess the influence of cell proximity on nanoparticle dynamics. These ranges were defined as 20-25µm, 45-50µm, 70-75µm and 95-100µm above the cell surface. Axial position was determined by systematic adjustment of the focal plane rather than by continuous 3D localisation of individual nanoparticles. Although defocus-based approaches can achieve sub-micron axial precision with appropriate calibration, the implementation used here prioritises experimental simplicity and compatibility with widefield microscopy. Consequently, nanoparticle positions along the axial dimension are represented as discrete ranges rather than precise z-coordinates.

The use of 5 µm ranges reflects the practical resolution of focal plane positioning while ensuring sufficient particle sampling within each region for robust statistical analysis. These ranges are

therefore interpreted as representing broad spatial zones above the cell surface, rather than precise axial localisations. The axial uncertainty associated with focal plane positioning is estimated to be approximately 1µm. For simplicity the maximum heights (25, 50, 75 and 100 µm) are used in the results section when referring to these regions. Prior to introducing the nanoparticles and tracking, the cells were washed with PBS to gently remove any vesicles or debris that could be mistaken for nanoparticles. Four independent samples were prepared, i.e., N=4 and six particles in each height range were tracked, i.e., n=6.

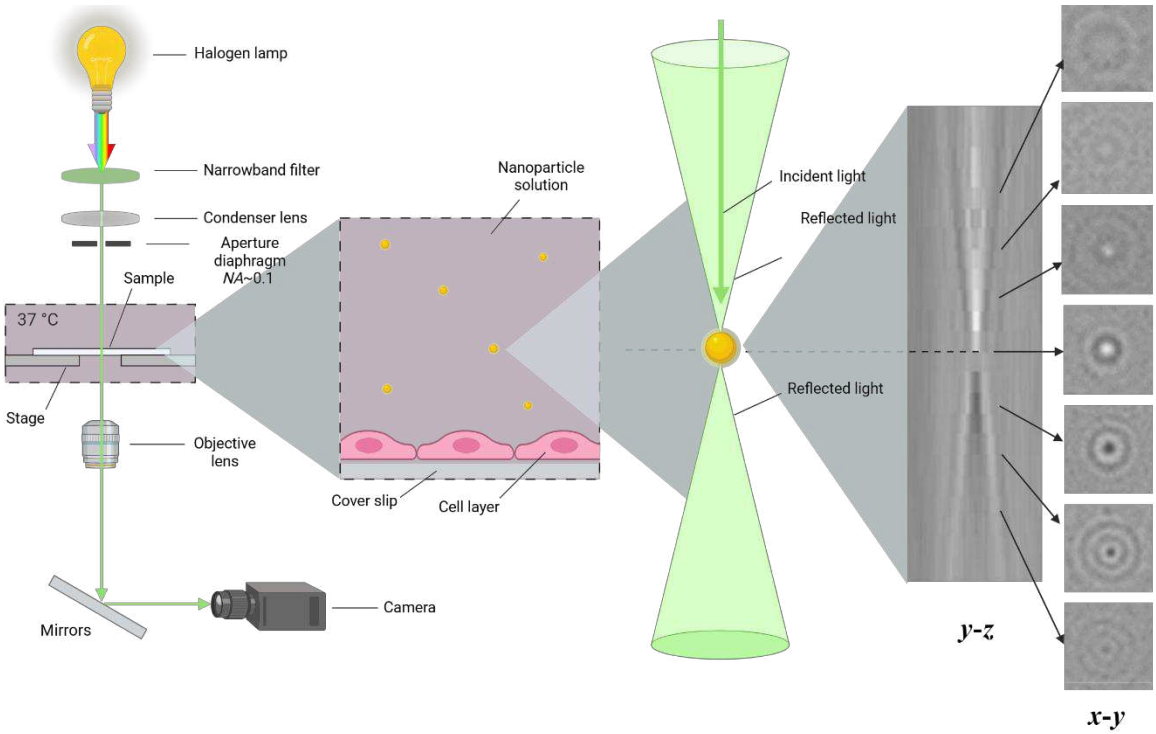


Figure 1: Nanoparticle visualisation methodology. Schematic of optical light path (left) used to generate caustic signature of small nanoparticles (right - adapted from [23]) above cells and position of nanoparticle relative to the caustics signature generated (centre, left). Created using BioRender.

Diffusion coefficient analysis

The experimental diffusion coefficient for a particle can be obtained from the mean square displacement (MSD) which quantifies the average squared distance travelled by a particle in a certain time [24]. In two dimensions, the MSD at the i^{th} position is expressed as follows [25]:

$$MSD = \frac{1}{N-n}\sum_{i=0}^{N-n}((\Delta x_i(\Delta t))^2 + (\Delta y_i(\Delta t))^2) \quad (1)$$

The mean square displacement, MSD can then be used to calculate an estimate of the diffusion coefficient from the experimental data, using the following expression:

$$D = \frac{MSD}{d(\Delta t)^{\alpha}} \quad (2)$$

where *d* is the number of dimensions (two in this study), *D* is the diffusion coefficient and Δ*t* is the time between frames and *α* is the anomalous diffusion coefficient.

The exponent α was obtained from a linear fit to the log–log plot of MSD versus τ. To minimise bias from statistical noise at long lag times, only the first 25 lag points were used for fitting. Normal diffusion is characterised by a linear relationship between the mean square displacement and time where $\alpha \sim 1$, thus anomalous diffusion is defined as $\alpha \neq 1$. There are various classes of anomalous diffusion but traditionally, it can be divided into at least two subcategories: superdiffusion when $\alpha > 1$ and subdiffusion when $\alpha < 1$. Statistical analysis was performed using a two-tailed Student's t-test, with significance defined as $p < 0.05$.

Stokes-Einstein diffusion equation

The Stokes-Einstein relationship was used to obtain an ideal reference point for particle diffusion in homogenous, simple media. The Stokes-Einstein diffusion coefficient has been calculated using the equation:

$$D_{SE} = \frac{K_b T}{6\pi\eta r} \quad (3)$$

where K_b is the Boltzmann constant, T and η are the temperature and viscosity of the solution and r is the radius of the particle of interest.

Convex hull analysis

A convex hull is the smallest convex polygon that can enclose all the random steps of the particle over the timesteps used to calculate the diffusion coefficient in two dimensions. It provides a measure of the spatial extent of the nanoparticle's movement in the x and y planes. The convex hull area is the total area covered by the nanoparticle over time. The convex hull was found using the convhull (convex hull) and polyarea (area of a polygon) functions in MATLAB.

Results and Discussion

Visibility of nanoparticles above cell layer

Gold nanoparticles as small as 20nm in diameter could be visualised above human mesenchymal stem cell (hMSC) monolayers (Figure S1) however tracking in real-time can comfortably be achieved with nanoparticles 50nm-100nm in diameter. Gold nanoparticles with diameters of 100nm were dispersed in Dulbecco's Modified Eagle medium (DMEM),

supplemented with and without fetal bovine serum (FBS), and tracked diffusing above a monolayer of human Mesenchymal Stem Cells (hMSCs). Nanoparticles could be tracked directly above the cell layer at a minimum distance of 25μm above the cell layer, as shown in Figure 2, at which distance the tracking software could easily distinguish the bright caustic signature produced by the nanoparticle separately from the signature produced by cells. Figure 3 shows the typical caustic signatures produced by the cell layer in DMEM with 10% FBS both with and without 100nm gold citrate nanoparticles. Cells imaged using the caustics technique without nanoparticles showed negligible sign of cell death up to two hours after being placed on a microscope slide and no trackable entities could be seen above 10μm from the surface of the cells. Cells exposed to nanoparticle solutions with and without the presence of FBS were viable up to 2 hours after nanoparticle exposure (Figure 4).

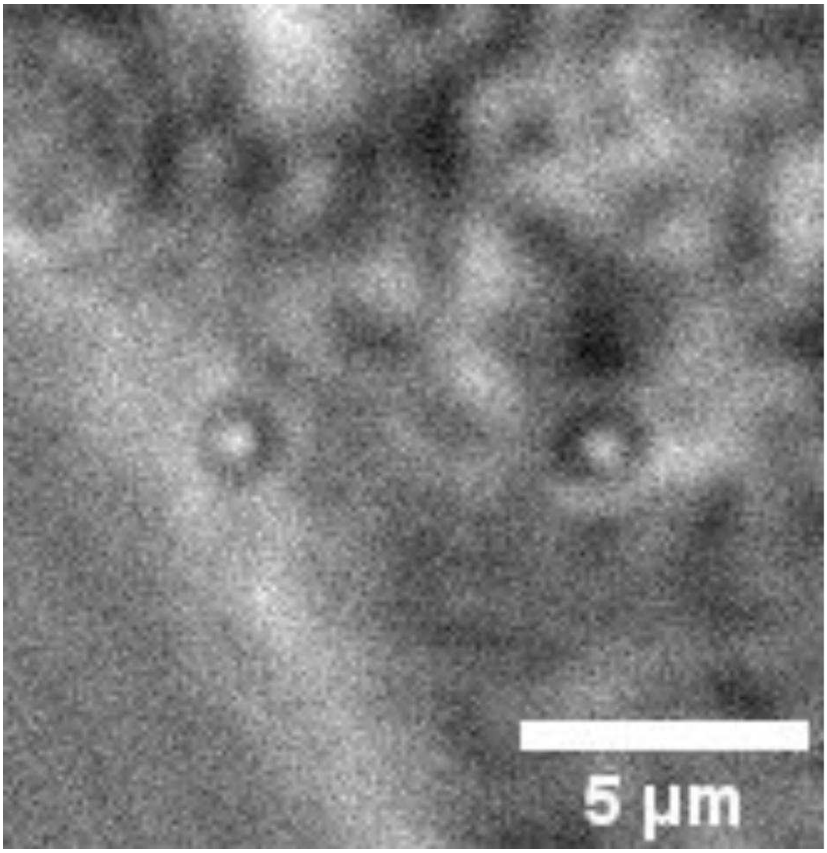


Figure 2: Nanoparticle caustic signatures above cells. Caustic signature of gold citrate-coated 100nm diameter nanoparticles 25μm above human mesenchymal stem cells.

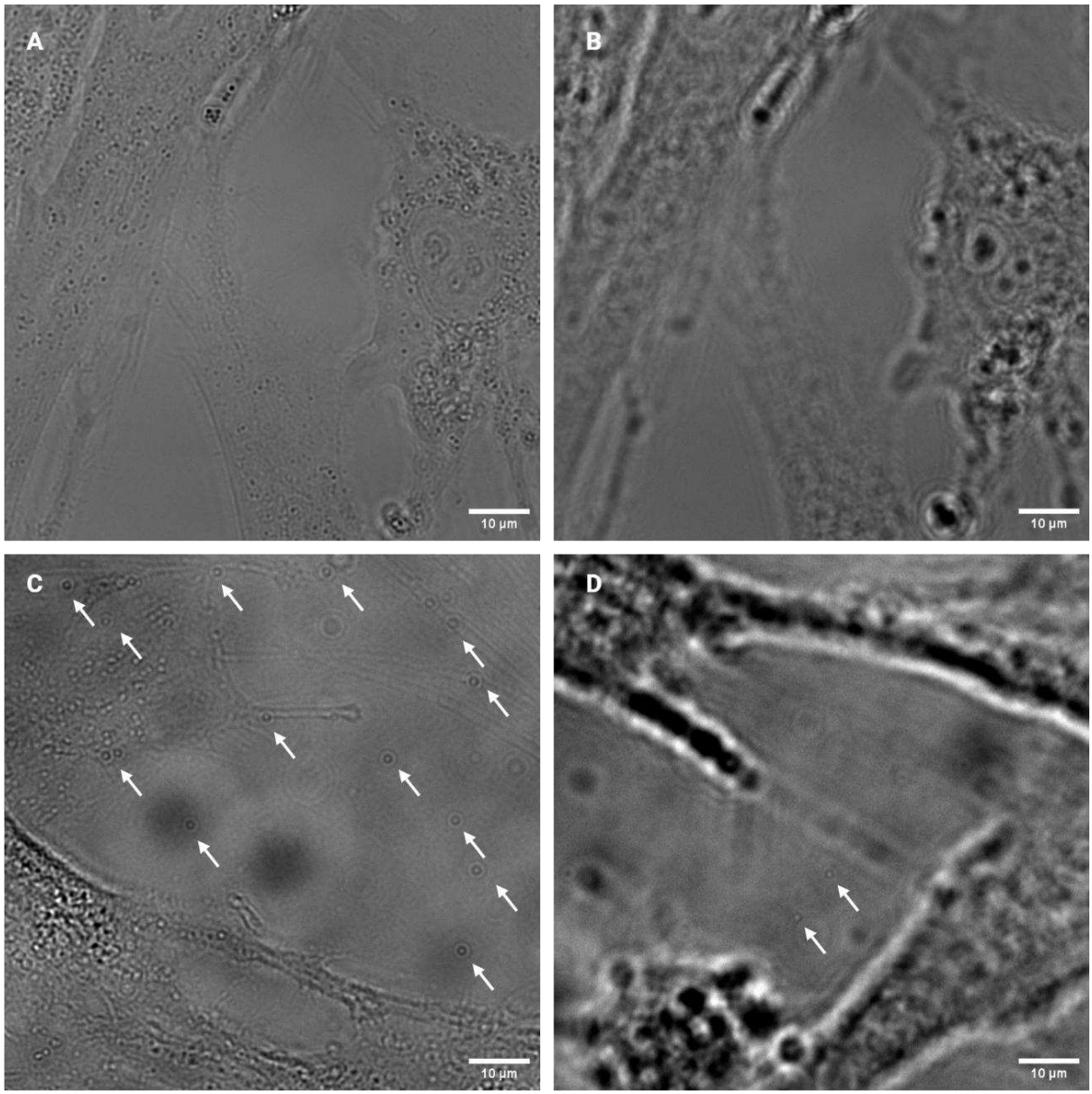


Figure 3: Caustic signatures of cells with and without nanoparticles. Images of Caustic signatures produced by human mesenchymal stem cells A.) without nanoparticles 0µm above the cells, B.) without nanoparticles 25µm above the cells, C.) with gold citrate 100nm diameter nanoparticles 0µm above the cells and D.) with gold citrate 100nm diameter nanoparticles 25µm above the cells. All images were taken 15-minutes after placement onto microscope slide cavity containing DMEM supplemented with 10% FBS and nanoparticle exposure.

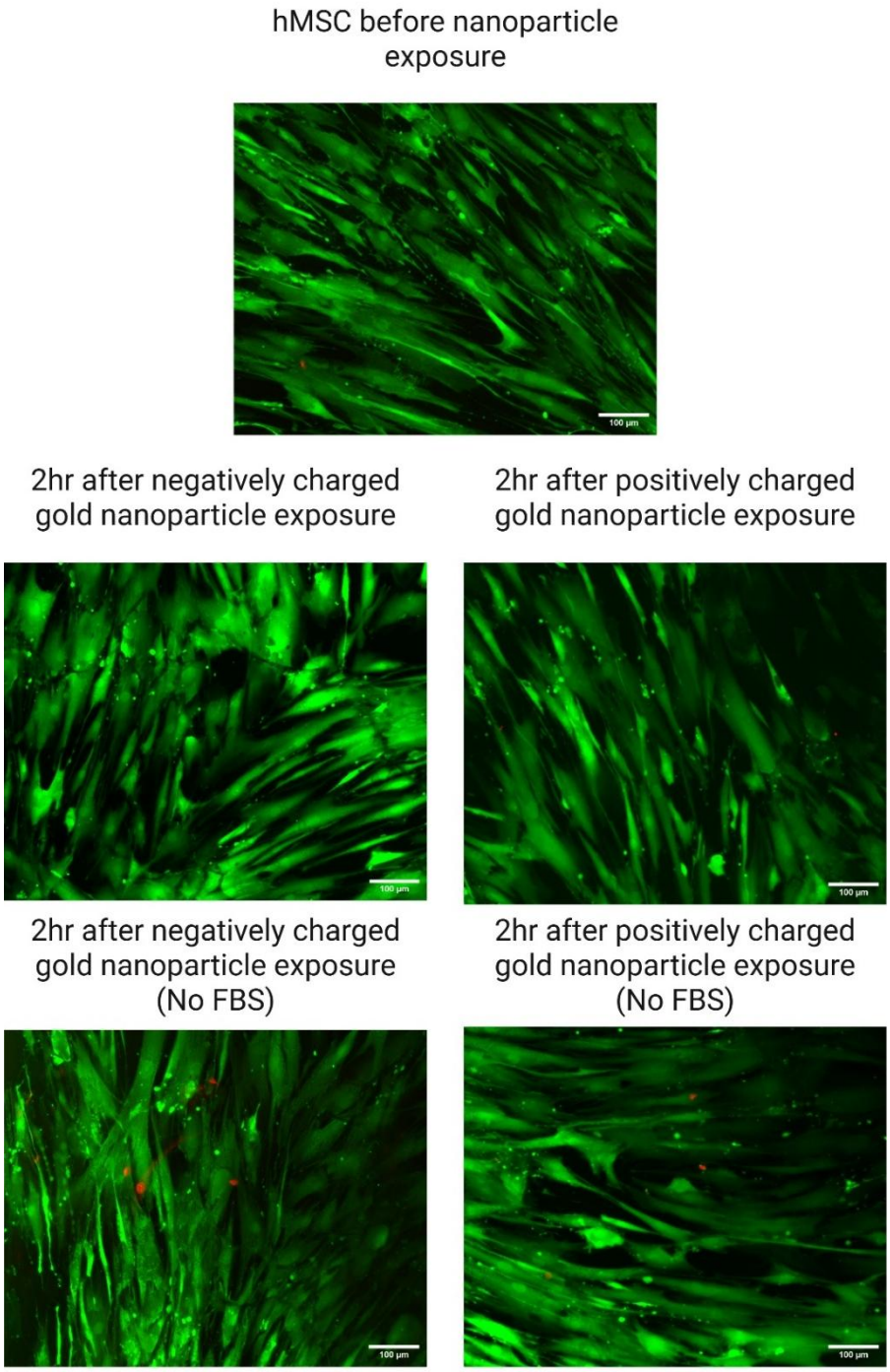


Figure 4: Human mesenchymal stem cells live/dead images. Representative images of human mesenchymal stem cells (hMSC) stained with a live/dead viability assay kit before nanoparticle exposure and 2 hours after exposure to citrate-coated and branched polyethylenimine (BPEI)- coated 100nm nanoparticle under tracking conditions. Assay shows negligible cell death after 2 hours of exposure to nanoparticles at concentrations used in tracking experiments.

Negatively charged nanoparticles do not show distance dependent behaviour at length scales used in the current study

Negatively charged gold nanoparticles (citrate) with a diameter of 100nm were tracked diffusing at different heights above hMSCs and their diffusion coefficients evaluated. Each average data point, box or bar presented in figures 5-11 represent averages of 24 measurements (6 measurements per replicate and total of 4 replicates for each experiment) and error bars in figures 5-7 and 11 represent a half standard deviation from the average. Fifteen minutes after exposure to the cell monolayer, nanoparticles dispersed in cell culture media with 10% FBS diffused at an approximately constant rate (Figure 5). The absence of FBS in the original nanoparticle solution did not have any significant effect on the diffusion rate of particles 15 minutes after exposure to the cell layer.

Diffusion behaviour of gold negatively charged gold nanoparticles with diameters of 137nm diffusing above mouse embryonic carcinoma (P19) cells in a study by Zhou et al using dark field microscopy showed a decrease in diffusion rate as nanoparticle approached the cell layer [26]. In the study by Zhou et al, three regions were identified in which nanoparticles exhibited distinct diffusion behaviour that was contradictory to the traditional view that there are two diffusion regimes in the vicinity of cells corresponding to when the nanoparticle is in the bulk media and on the cell membrane. The additional region was identified as the pericellular matrix, a specialized region of the extracellular matrix several microns thick. The transition between the diffusion behaviour of particles in the bulk media and slowed diffusion in the pericellular matrix occurred approximately 8μm away from the cell layer. In the present study, nanoparticles have been tracked at greater distances from the cell layer than the thickness of most reported pericellular matrices [26-28]. It can therefore be assumed that nanoparticles are in contact with the cell-conditioned medium and any changes in diffusion are potentially as a result of biological interactions within this environment rather than direct interaction with extracellular matrix.

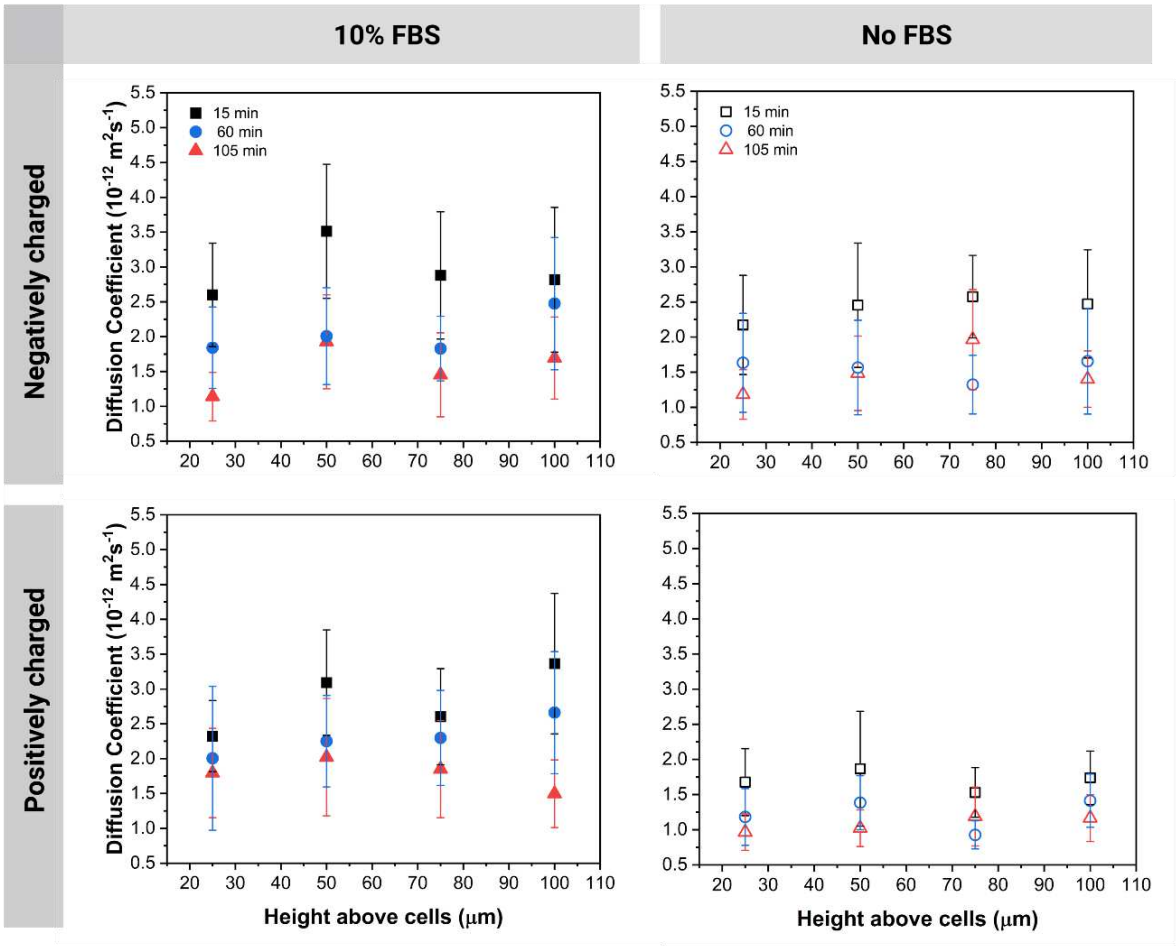


Figure 5: Diffusion coefficients of nanoparticles as function of height above cells. Average values of experimental diffusion coefficient for negatively- (left) and positively- (right) charged gold nanoparticles in DMEM with 10% FBS and no FBS with a diameter of 100nm as a function of their height above a cell monolayer, tracked over time. Error bars represent a half s.d. from the mean (N = 4).

Time dependence of negatively charged nanoparticle dynamics above cells

The diffusion coefficients of negatively charged (citrate) nanoparticles in DMEM with 10% FBS found diffusing in each of the different regions above the cell layer decreased over time (Figure 6). 105 minutes after exposure to the cell layer, nanoparticles found throughout the media (25μm -100μm above the cell layer) diffused at a significantly slower, constant rate compared to 15 minutes after exposure to the cell layer (25μm: $p<0.001$; 50μm: $p=0.0022$; 75μm: $p=0.0030$; 100μm: $p=0.029$).

Protein corona formation and composition are rapidly established when nanoparticles are incubated with human plasma [29]. It can be assumed that before the first diffusion measurement, a protein corona has already formed on these nanoparticles. However, the

secretion of small biomolecules and proteins into the extracellular environment by cells can induce dynamic changes in the protein corona through protein exchange or rearrangement [17,30]. The ‘hard corona’ composed of strongly bound proteins, develops over timescales of minutes to hours as higher-affinity interactions progressively displace more weakly associated species. In contrast a ‘soft corona’ of loosely bound proteins remains in continuous dynamic exchange with the surrounding environment [31,32]. Over the course of nanoparticle tracking in the present study, it is possible that corona composition evolved dynamically, potentially contributing to the observed changes in diffusion behaviour.

UV–vis spectroscopy (data not shown) was inconclusive for detecting changes in bulk protein concentration in the media over time, suggesting that any variations affecting nanoparticle dynamics occur below the detection limit or are localised at the nanoparticle interface. A limitation of this study is that protein–nanoparticle interactions are inferred rather than directly measured.

Recent advances in single-particle, label-free techniques have enabled in situ investigation of protein corona formation. Approaches such as real-time 3D single-particle tracking spectroscopy (RT-3D-SPT) [33], differenced resonance light scattering correlation spectroscopy (D-RLSCS) [34] and real-time all-optical nanoparticle analysis by scattering microscopy (RONAS) [35] are capable of probing adsorption dynamics at the single-particle level. These methods provide valuable insights into corona formation and evolution in complex media. However, they typically require specialised instrumentation, active particle tracking, or highly controlled experimental conditions, which can limit their applicability in widefield measurements in heterogeneous cellular environments.

Consequently, protein corona characterisation is still frequently performed ex situ, where nanoparticle-protein complexes are isolated from their native environment. Such approaches can perturb weakly bound (‘soft’) corona components through washing, dilution, or shear forces [36]. Moreover, both in situ and ex situ methods may provide only partial representations of the dynamic and spatially heterogeneous conditions experienced by nanoparticles during interaction with living cells [36,37]. Consequently, the precise relationship between corona evolution and nanoparticle dynamics in the pericellular environment remains challenging to resolve directly.

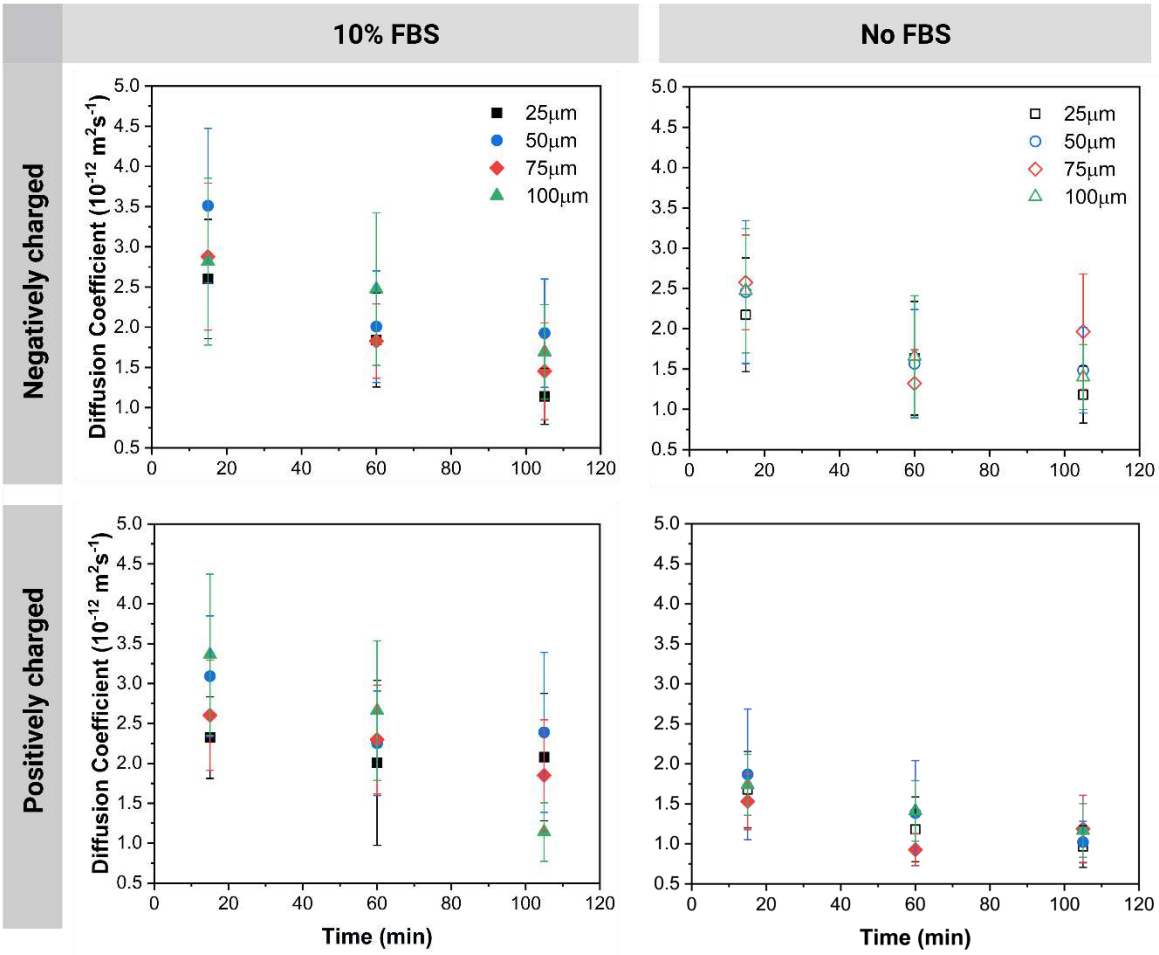


Figure 6: Diffusion coefficients of nanoparticles as function of time. Average values of experimental diffusion coefficient for negatively- (top) and positively (bottom) charged gold nanoparticles in DMEM with 10% FBS (left) and no FBS (right) with a diameter of 100nm as a function of time after cell exposure. Negatively charged nanoparticles in DMEM with 10% FBS displayed the greatest reduction in diffusion coefficient over time. Error bars represent a half s.d. from the mean (N = 4).

Absence of serum proteins has a significant effect on positively charged nanoparticle dynamics

Gold positively charged (BPEI) nanoparticles with diameters of 100nm were also tracked above the hMSC monolayer and their diffusion coefficients evaluated (Figure 5). The absence of FBS in the media resulted in significantly lower diffusion coefficients for the positively charged nanoparticles 15 minutes after exposure to the cells at all heights above the cells (25µm: $p=0.032$; 50µm: $p=0.011$; 75µm: $p=0.0065$; 100µm: $p=0.013$), at 60 minutes at some heights (50µm: $p=0.0089$; 75µm: $p<0.001$; 100µm: $p=0.0029$) and 105 minutes at some heights (25µm: $p=0.0062$; 50µm: $p=0.0093$) compared to nanoparticles in the presence of FBS. Positively

charged nanoparticles also exhibited a decrease in their diffusion rate after 105 minutes compared to the initial measurements in both DMEM with FBS and without FBS. In DMEM with FBS the decrease was significant at 50μm and 100μm above the cells (50μm: $p=0.028$; 100μm: $p<0.001$) and in DMEM with no FBS the decrease was significant at 25μm, 50μm and 100μm above the cells (25μm: $p=0.0029$; 50μm: $p=0.022$; 100μm: $p=0.0097$.)

Charge plays a role in the interactions between nanoparticles and proteins. According to current literature, positively charged nanoparticles adsorb a higher quantity of proteins than negatively charged nanoparticles due to strong electrostatic interactions between the nanoparticles and serum proteins. However, negatively charged nanoparticles still adsorb some quantity of proteins [38]. The differences in dynamics seen between the positively- and negatively- charged nanoparticles could also be due to the type of proteins adsorbed. Positive and negatively charged surfaces, due to electrostatic interactions, attract and bind different proteins resulting in unique corona compositions and potentially a different biological response [39].

Additionally, both the positively and negatively charged nanoparticles in DMEM with 10% FBS can be assumed to be coated with serum proteins as protein adsorption is an instantaneous process and will occur before the first data point at 15 minutes [40], hence potentially having an impact on the biological interaction of nanoparticles upon exposure to cells. The presence of a serum protein corona on nanoparticles in DMEM with 10% FBS appears to reduce the effect of the cell layer on the diffusion of positively charged nanoparticles, allowing nanoparticles with a pre-formed corona to diffuse at a faster rate above the cells than nanoparticles in DMEM without FBS which could indicate the response of nanoparticles after contact with physiological fluids or following functionalisation with a protein coating.

The presence of cells affects the in vitro dynamics of nanoparticles

Negatively (citrate) and positively (BPEI) charged nanoparticles with diameters of 100nm were tracked in DMEM with and without FBS, diffusing 50μm above a cell-free glass surface, 15 and 105 minutes after sample preparation (Figure 7). The dynamics of negatively charged particles in the presence of cells are significantly different from those observed in cell-free conditions. After 105 minutes, negatively charged particles in the absence of cells show no significant decrease in diffusion rate, suggesting that the slower dynamics observed near cells arise from cellular proteins, extracellular matrix components, or cell-mediated sensing. Similarly, positively charged nanoparticles in DMEM with 10% FBS exhibit no reduction in diffusion coefficient when cells are absent. Positively charged nanoparticles in DMEM without FBS initially diffuse at rates

comparable to those in the protein-containing medium; however, no particles remained diffusing freely above the glass surface after 105 minutes and their average diffusion coefficient is represented as zero in figure 7. Over the tracking period, these nanoparticles were observed to become adhered to the glass, likely due to strong electrostatic attraction and van der Waals forces between the positively charged particles and the negatively charged glass surface. In comparison, the presence of serum proteins shields the positive surface charge of the nanoparticles, reducing their effective charge and preventing surface adhesion, which allows the particles to remain in suspension after 105 minutes.

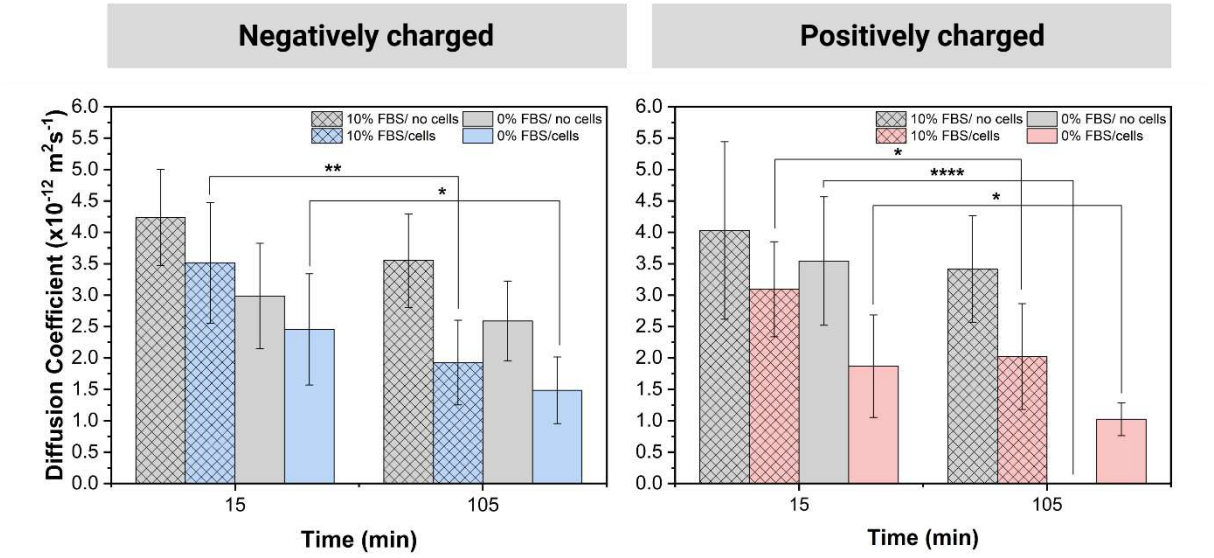


Figure 7: Diffusion coefficients of nanoparticles in the presence and absence of cells. Experimental diffusion coefficient for negatively- and positively-charged gold nanoparticles with a diameter of 100nm in DMEM with 10% FBS and no FBS both in the presence (colour) and absence (grey) of cells as a function of time after exposure to cell/control surface, tracked 50μm above the surface (* p<0.05, **p<0.01, ***p<0.001, ****p<0.0001). Error bars represent a half s.d. from the mean (N = 4).

Evolution of the effective transport environment

The Stokes-Einstein equation predicts a diffusion coefficient of 4.88 μm^2 s^{-1} for a 100 nm particle in DMEM supplemented with 10% FBS (Table 1). Experimental measurements in the absence of cells were lower than this prediction, consistent with previous observations that nanoparticles at low concentrations (similar to those used in the current study), below a certain threshold size exhibit departures from classical Stokes-Einstein behaviour when examined using this tracking methodology [20]. Consequently, the Stokes-Einstein prediction is treated here as an ideal transport reference rather than a strict expectation for nanoparticle motion.

Table 2 presents average experimental values of nanoparticle diffusion 50μm above the cells or glass surface. As has already been mentioned, the introduction of living cells produced an additional reduction in diffusivity. The initial diffusion coefficients measured 15 minutes after exposure to cells were 40%-65% lower than the corresponding Stokes-Einstein prediction, indicating that nanoparticle transport in the extracellular environment differs substantially from ideal Brownian transport in a homogeneous fluid.

Table 1: Theoretical Stokes-Einstein diffusion coefficients. Theoretical Stokes-Einstein diffusion coefficient values of 100nm nanoparticles in solutions at 37°C.

Condition	**Diffusion coefficient ($\mu m^2/s$)**
Water, 37°C	6.59
DMEM, 37°C	6.21
DMEM + 10% FBS, 37°C	4.88

Table 2: Experimental diffusion coefficients. Average experimental diffusion coefficient values of 100nm nanoparticles in solutions at 37°C, 15 minutes after cell and cell culture media exposure. Values are given for particles 50 μm above cell or glass surface.

	Diffusion coefficient ($\mu m^2/s$)			
Charge	*DMEM*	*DMEM + 10% FBS*	*DMEM + hMSC*	*DMEM + 10% FBS + hMSC*
-	3.54	4.24	2.45	3.51
+	2.99	4.02	1.87	3.09

Three transport states can potentially be seen from the data: 1.) Ideal transport predicted with the Stokes-Einstein theory (Table 1), 2.) effective transport in cell-free biological media (Table 2, data columns 1-2) and 3.) cell-conditioned transport in the presence of living cells (Table 2, data columns 3-4). Protein corona formation is expected to modify nanoparticle hydrodynamic size and therefore diffusivity. Previous studies have reported increases in hydrodynamic diameter of approximately 30% for negatively charged gold nanoparticles following incubation in DMEM supplemented with serum proteins [41]. However, protein adsorption occurs rapidly and is likely to be mostly established before the first measurements were taken. The experimentally measured diffusivity of nanoparticles in DMEM with and without FBS decreased by approximately 15%-19% during the 105-minute exposure to the cellular environment. This

suggests that nanoparticle transport is sensitive to continuing changes in the local extracellular environment.

Alpha exponent analysis

The anomalous diffusion exponent, α, was determined for individual nanoparticles by fitting a linear model to the logarithmic relationship between the MSD and τ. For each sample, the mean α value at a given height above the cell layer remained approximately constant, with no systematic variation observed between experimental conditions, including the presence of FBS or particle surface charge (Figure 8). In each graph, the ensemble-averaged α is indicated as a horizontal red line and is close to 1 for all conditions. Data that fell outside 1.5 times the interquartile range (IQR) has been exclude from figure 8 but can be seen in the supplementary material (Figure S2 and S3).

An average α value of approximately 1 suggests that at the ensemble level, nanoparticle transport in these biological media conditions is consistent with Brownian diffusion despite progressively decreasing diffusion coefficients over time. However, a broad and reproducible distribution of α values were observed for individual particles within each sample. It was found that 75.69%-82.99% of α values for all nanoparticles tracked fell within the range $0.75 < \alpha < 1.25$. The wide distribution of α values could indicate the influence of local microenvironmental factors on individual trajectories, rather than a single, uniform diffusion mechanism.

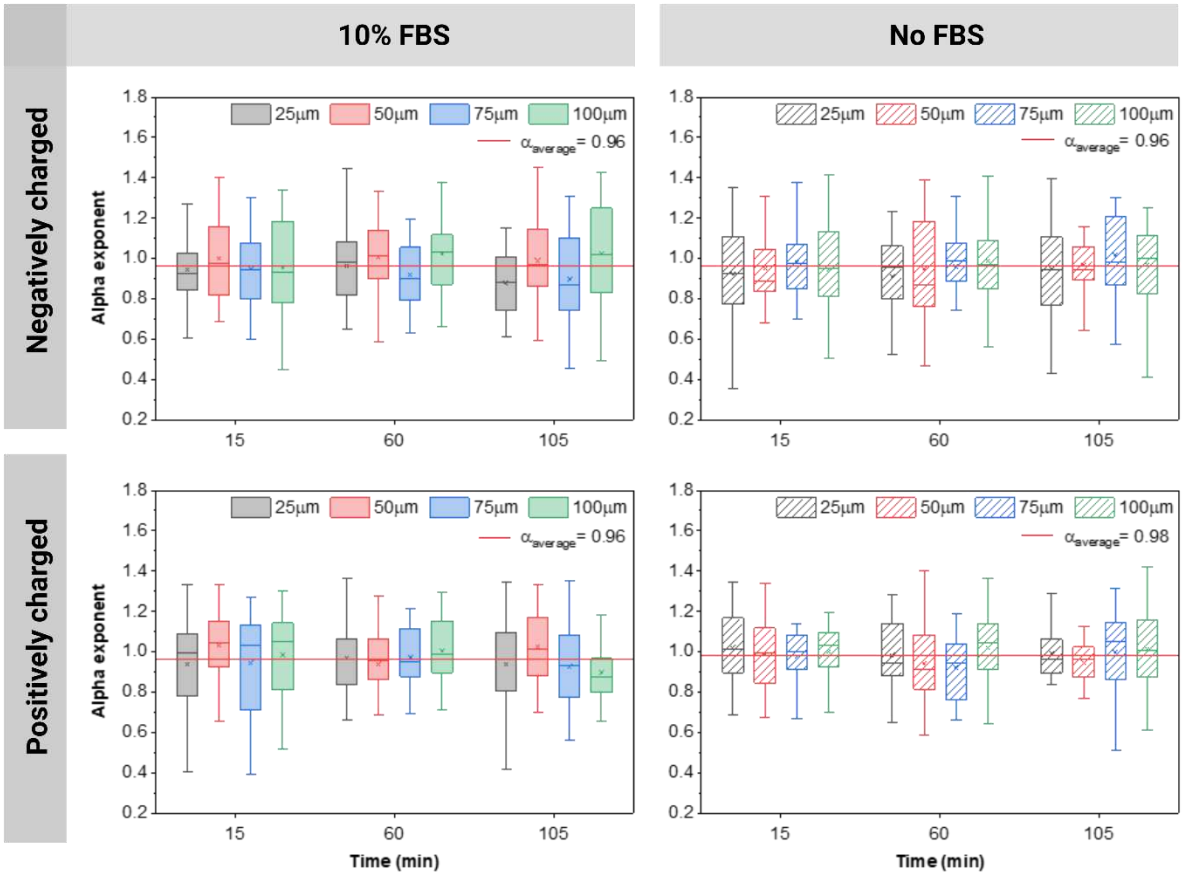


Figure 8: Alpha exponent of nanoparticle trajectories. Average anomalous alpha exponent for negatively- and positively charged gold nanoparticles with a diameter of 100nm in DMEM with 10% FBS and no FBS above a cell monolayer. Box represents the interquartile range (IQR), with the mean marked by an empty square and median marked by a line within the box. Whiskers extend to the most extreme data points within 1.5 times the IQR (N = 4). Data outside this range has been excluded from this graph.

Convex hull area analysis

Figure 9 shows the convex hull area of negatively charged 100nm gold nanoparticles in DMEM with 10% FBS and without FBS at 15-, 60- and 105-minutes after exposure to the cell layer. 15 minutes after exposure to cells, nanoparticles both in the presence and absence of FBS displayed a large scatter in the convex hull area, with no significant difference between the average values calculated for particles in each height range above the cells. Over time, the average convex hull area decreases as the diffusion rate of nanoparticles also decreases, implying that the area over which particles are traveling in two dimensions also decreases. The decrease in average convex hull area over time could suggest more particles are interacting at a localized level with biological components of the media. These results could indicate that there

is an increased proportion of nanoparticles becoming 'trapped' in the media and therefore, not reaching a target site.

Positively charged nanoparticles in DMEM with 10% FBS also show a wide scatter in values for their convex hull area (Figure 10). The wide distribution of areas is suggestive of a heterogeneous solution where nanoparticles are both interacting with biological components in a localized environment leading to a smaller convex hull area and diffusing freely over wider areas giving larger convex hull areas. Positively charged nanoparticles in DMEM with no FBS show a much smaller distribution of areas therefore, from the data it can be said that the combination of nanoparticle characteristics and media conditions impact the uniformity of diffusion.

Negatively charged nanoparticles tracked 50µm above a glass surface in the absence of cells displayed no significant change in their measured convex hull areas over time in both DMEM with and without FBS demonstrating the effect of the cell layer on the spatial dynamics of gold nanoparticles (Figure 11). Similarly, positively charged nanoparticles dispersed in DMEM with 10% FBS in the absence of cells showed no significant change in the measured convex hull area over time and no data is available for nanoparticles in DMEM without FBS. Convex hull area analysis could give an indication of how nano and micro entities are interacting in a heterogeneous solution. This variability in diffusion behaviour is consistent with trends observed in the α exponent analysis, which also indicated broad trends in transport modes within the nanoparticle population.

On a final note, in combination with diffusion coefficient analysis, we have experimentally determined nanoparticle dynamic behaviour in biologically relevant environments. The results presented show that multiple factors could be contributing to changes in nanoparticle dynamics on approach to a cell layer. The heterogeneous nature of biological environments could lead to nanoparticles exhibiting several diffusive behaviours within one population. The diffusion analysis used in this study employs a deliberately simple MSD-based framework to extract diffusion coefficients and anomalous exponents, enabling clear comparison across conditions. Enhancements to the experimental methodology, such as longer observation times or increased trajectory counts, would improve statistical confidence and enable more detailed, time-resolved analyses. The use of an accessible and widely applicable experimental and analytical approach can however establish a reproducible baseline for nanoparticle diffusion under biologically relevant conditions, thus providing a strong foundation for future

enhancement of the caustics microscopy technique and investigation of transport regimes in biological media.

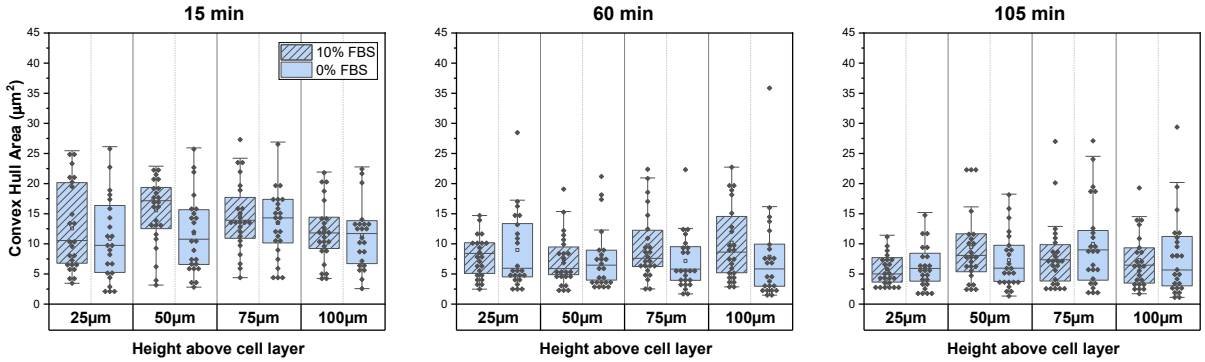


Figure 9: Convex hull areas of negatively charged nanoparticles. Convex hull areas of negatively charged gold citrate nanoparticles with a diameter of 100nm, measured A.) 15-minutes, B.) 60-minutes and C.) 105-minutes after exposure to a cell monolayer, as a function of their height above the cell monolayer. Box represents the interquartile range (IQR), with the mean marked by an empty square and median marked by a line within the box. Whiskers extend to the most extreme data points within 1.5 times the IQR (N = 4).

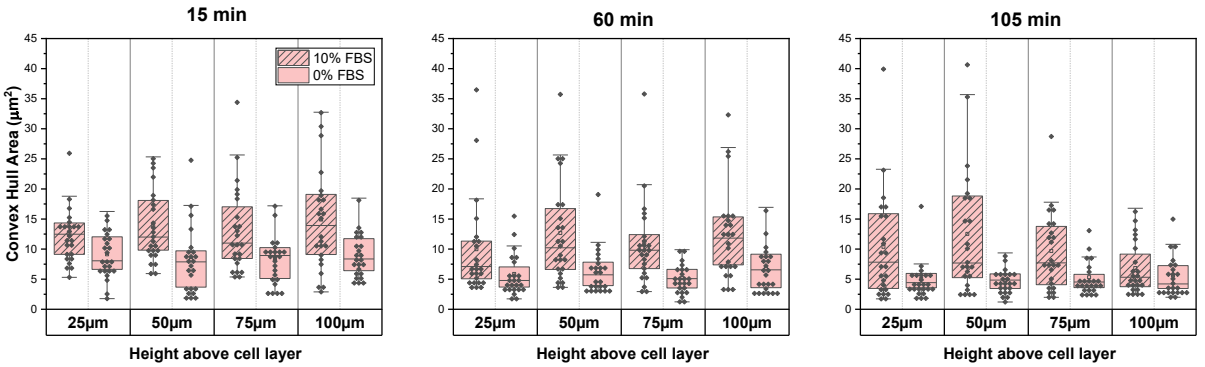


Figure 10: Convex hull areas of positively charged nanoparticles. Convex hull areas of positively-charged gold BPEI nanoparticles with a diameter of 100nm, measured A.) 15-minutes, B.) 60-minutes and C.) 105-minutes after exposure to a cell monolayer, as a function of their height above the cell monolayer. Box represents the interquartile range (IQR), with the mean marked by an empty square and median marked by a line within the box. Whiskers extend to the most extreme data points within 1.5 times the IQR (N = 4).

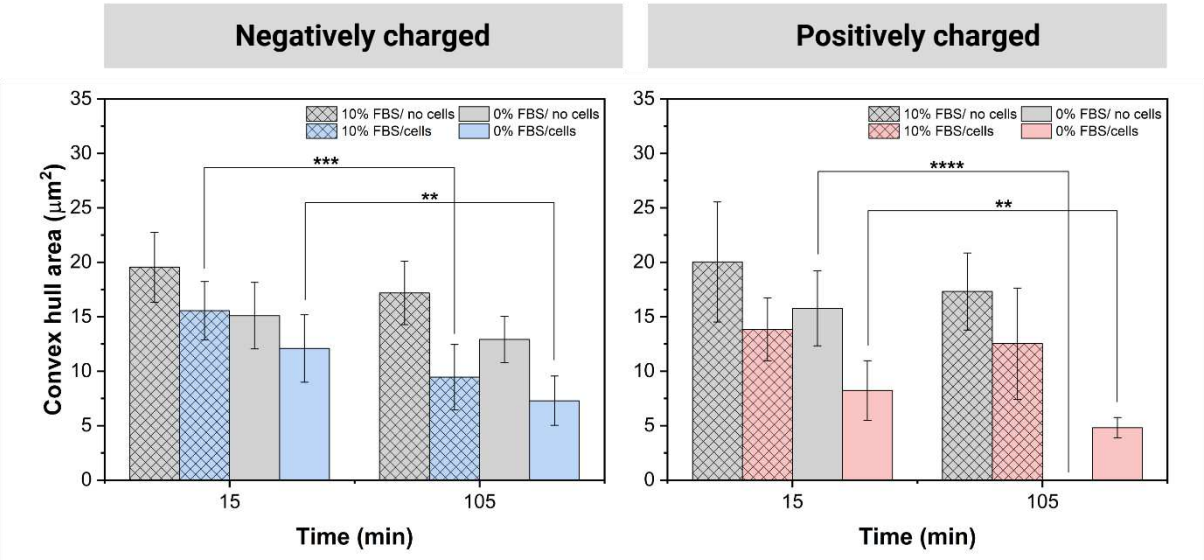


Figure11: Convex hull areas of nanoparticles in the presence and absence of cells. Convex hull area for negatively- and positively-charged gold nanoparticles with a diameter of 100nm in DMEM with 10% FBS and no FBS both in the presence (colour) and absence (grey) of cells as a function of time after exposure to cell/control surface, tracked 50μm above the surface (* p<0.05, **p<0.01, ***p<0.001, ****p<0.0001). Error bars represent a half s.d. from the mean (N = 4).

Conclusions

A technique initially developed to track synthetic nanoparticles in simple solutions has been successfully applied to tracking metallic nanoparticles in complex biological environments in the presence of live cells as an exemplar for the behaviour of nanoscale entities. Both positively- and negatively charged gold nanoparticles were dispersed in DMEM (Dulbecco's Modified Eagle medium), with and without the addition of FBS (fetal bovine serum) and exposed to Human Mesenchymal Stem Cells. The values of diffusion coefficient, anomalous alpha exponent and convex hull area of these nanoparticles at different heights above a cell monolayer were experimentally derived from measurements of their random tracks and potentially reveal information about the microenvironments near the cells. Experimental diffusion coefficients were compared to diffusion coefficients determined from the Stokes-Einstein theory. This showed that experimental diffusion behaviour deviated considerable from idealised behaviour. We have also demonstrated that nanoparticle dynamics in biological media are governed by physicochemical properties, such as particle surface charge, and *in vitro* conditions. The results from this study suggest that potential changes in media composition over time due to cellular activity can have a significant impact on nanoparticle diffusivity whilst the averaged anomalous diffusion exponent remained close to 1. This indicated that, at the

ensemble level, nanoparticles exhibited normal diffusive behaviour. This could potentially suggest that the extracellular environment modifies the rate of transport rather than inducing strongly anomalous diffusion. Finally, we have demonstrated the capability of an accessible, label-free optical technique to visualise and track nanoparticles directly above cell layers which could be used to gain information on the ability of nanoparticles to diffuse in complex environments.

Author contributions

G.S. performed the experiments, analysed the data and prepared the first draft of the manuscript; J.M.C. and E.A.P. conceived, coordinated and supervised the study, participated in the interpretation of the results and edited the manuscript. All authors gave final approval for publication.

Funding

G.S. was supported by the Biotechnology and Biological Sciences Research Council (BBSRC) and is part of the Collaborative Training Partnership in which the BBSRC is supported by a number of industrial partners.

Data availability

The datasets generated and/or analysed during the current study are available in the DataCat repository at: https://datacat.liverpool.ac.uk/id/eprint/3041

Competing interests

The authors declare no competing interests.

References

1 Coppens, B. *et al.* Anomalous diffusion of nanoparticles in the spatially heterogeneous biofilm environment. *iScience* **26**, doi:10.1016/j.isci.2023.106861 (2023).

2 Zhang, X. *et al.* Enhancement and characterization of nanoparticle diffusion in biological tissues by magnetic heating and oscillation. *Journal of Controlled Release* **380**, 725-735, doi:https://doi.org/10.1016/j.jconrel.2025.02.023 (2025).

3 Zhou, R., Zhou, H., Xiong, B., He, Y. & Yeung, E. S. Pericellular Matrix Enhances Retention and Cellular Uptake of Nanoparticles. *Journal of the American Chemical Society* **134**, 13404-13409, doi:10.1021/ja304119w (2012).

4 Xu, R. *et al.* Pericellular matrix plays an active role in retention and cellular uptake of large-sized nanoparticles. *Analytical and bioanalytical chemistry* **406**, 5031-5037 (2014).

5 Al-Obaidi, H. & Florence, A. T. Nanoparticle delivery and particle diffusion in confined and complex environments. *Journal of Drug Delivery Science and Technology* **30**, 266-277, doi:https://doi.org/10.1016/j.jddst.2015.06.017 (2015).

6 Mun, E. A. *et al.* On the role of specific interactions in the diffusion of nanoparticles in aqueous polymer solutions. *Langmuir* **30**, 308-317, doi:10.1021/la4029035 (2014).

7 He, X. *et al.* Extracellular matrix physical properties govern the diffusion of nanoparticles in tumor microenvironment. *Proceedings of the National Academy of Sciences* **120**, e2209260120, doi:doi:10.1073/pnas.2209260120 (2023).

8 Manzo, C. & Garcia-Parajo, M. F. A review of progress in single particle tracking: from methods to biophysical insights. *Rep Prog Phys* **78**, 124601, doi:10.1088/0034-4885/78/12/124601 (2015).

9 Huang, S. & Huang, G. The utilization of quantum dot labeling as a burgeoning technique in the field of biological imaging. *RSC advances* **14**, 20884-20897 (2024).

10 Giorgi, F., Curran, J. M. & Patterson, E. A. Real-time monitoring of the dynamics and interactions of bacteria and the early-stage formation of biofilms. *Scientific Reports* **12**, 1-14 (2022).

11 Wang, F. *et al.* Scattered Light Imaging Enables Real-Time Monitoring of Label-Free Nanoparticles and Fluorescent Biomolecules in Live Cells. *Journal of the American Chemical Society* **141**, 14043-14047, doi:10.1021/jacs.9b05894 (2019).

12 Thomsen, T., Ayoub, A. B., Psaltis, D. & Klok, H.-A. Fluorescence-Based and Fluorescent Label-Free Characterization of Polymer Nanoparticle Decorated T Cells. *Biomacromolecules* **22**, 190-200, doi:10.1021/acs.biomac.0c00969 (2021).

13 Taylor, R. W. & Sandoghdar, V. Interferometric Scattering Microscopy: Seeing Single Nanoparticles and Molecules via Rayleigh Scattering. *Nano Letters* **19**, 4827-4835, doi:10.1021/acs.nanolett.9b01822 (2019).

14 Huang, Y.-F. *et al.* Coherent Brightfield Microscopy Provides the Spatiotemporal Resolution To Study Early Stage Viral Infection in Live Cells. *ACS Nano* **11**, 2575-2585, doi:10.1021/acsnano.6b05601 (2017).

15 You, X. *et al.* Large field-of-view plasmonic scattering imaging and sensing of nanoparticles with isotropic point-spread-function. *Nature Communications* **16**, 5104, doi:10.1038/s41467-025-60460-7 (2025).

16 Lasne, D. *et al.* Single nanoparticle photothermal tracking (SNaPT) of 5-nm gold beads in live cells. *Biophysical journal* **91**, 4598-4604 (2006).

17 Ge, F., Xue, J., Du, Y. & He, Y. Unmodified single nanoparticles undergo a motion-pattern transition on the plasma membrane before cellular uptake. *Nano Today* **39**, 101158, doi:https://doi.org/10.1016/j.nantod.2021.101158 (2021).

18 Chen, S. *et al.* Label free imaging and deep tracking of single biological nanoparticles in free solution by reflection enhanced dark field scattering microscopy. *Sensors and Actuators B: Chemical* **355**, 131317, doi:https://doi.org/10.1016/j.snb.2021.131317 (2022).

19 Patterson, E. A. & Whelan, M. P. Tracking nanoparticles in an optical microscope using caustics. *Nanotechnology* **19**, 105502, doi:10.1088/0957-4484/19/10/105502 (2008).

20 Coglitore, D., Edwardson, S. P., Macko, P., Patterson, E. A. & Whelan, M. Transition from fractional to classical Stokes–Einstein behaviour in simple fluids. *Royal Society open science* **4**, 170507 (2017).

21 Schleyer, G., Patterson, E. A. & Curran, J. M. Label free tracking to quantify nanoparticle diffusion through biological media. *Scientific reports* **14**, 18822 (2024).

22 Gill, G. W. in *Cytopreparation: Principles & Practice* 309-323 (Springer, 2012).

23 Patterson, E. A. & Whelan, M. P. Optical signatures of small nanoparticles in a conventional microscope. *Small* **4 10**, 1703-1706 (2008).

24 Schirripa Spagnolo, C. & Luin, S. Trajectory Analysis in Single-Particle Tracking: From Mean Squared Displacement to Machine Learning Approaches. *International Journal of Molecular Sciences* **25**, 8660 (2024).

25 Michalet, X. Mean square displacement analysis of single-particle trajectories with localization error: Brownian motion in an isotropic medium. *Physical Review E* **82**, 041914, doi:10.1103/PhysRevE.82.041914 (2010).

26 Zhou, R., Xiong, B., He, Y. & Yeung, E. S. Slowed diffusion of single nanoparticles in the extracellular microenvironment of living cells revealed by darkfield microscopy. *Analytical and bioanalytical chemistry* **399**, 353-359 (2011).

27 Evanko, S. P., Tammi, M. I., Tammi, R. H. & Wight, T. N. Hyaluronan-dependent pericellular matrix. *Advanced Drug Delivery Reviews* **59**, 1351-1365, doi:https://doi.org/10.1016/j.addr.2007.08.008 (2007).

28 Nijenhuis, N., Mizuno, D., Spaan, J. A. & Schmidt, C. F. High-resolution microrheology in the pericellular matrix of prostate cancer cells. *J R Soc Interface* **9**, 1733-1744, doi:10.1098/rsif.2011.0825 (2012).

29 Tenzer, S. *et al.* Rapid formation of plasma protein corona critically affects nanoparticle pathophysiology. *Nature Nanotechnology* **8**, 772-781, doi:10.1038/nnano.2013.181 (2013).

30 Albanese, A. *et al.* Secreted biomolecules alter the biological identity and cellular interactions of nanoparticles. *ACS Nano* **8**, 5515-5526, doi:10.1021/nn4061012 (2014).

31 Vroman, L., Adams, A., Fischer, G. & Munoz, P. Interaction of high molecular weight kininogen, factor XII, and fibrinogen in plasma at interfaces. (1980).

32 Dawson, K. A. & Yan, Y. Current understanding of biological identity at the nanoscale and future prospects. *Nature nanotechnology* **16**, 229-242 (2021).

33 Tan, X. & Welsher, K. Particle-by-Particle In Situ Characterization of the Protein Corona via Real-Time 3D Single-Particle-Tracking Spectroscopy. *Angewandte Chemie International Edition* **60**, 22359-22367, doi:https://doi.org/10.1002/anie.202105741 (2021).

34 Zhang, T., Dong, C. & Ren, J. Probing the Protein Corona of Nanoparticles in a Fluid Flow by Single-Particle Differenced Resonance Light Scattering Correlation Spectroscopy. *Anal Chem*, doi:10.1021/acs.analchem.2c04568 (2023).

35 Dolci, M. *et al.* Real-Time Optical Tracking of Protein Corona Formation on Single Nanoparticles in Serum. *ACS Nano* **17**, 20167-20178, doi:10.1021/acsnano.3c05872 (2023).

36 Weber, C., Morsbach, S. & Landfester, K. Possibilities and limitations of different separation techniques for the analysis of the protein corona. *Angewandte Chemie International Edition* **58**, 12787-12794 (2019).

37 Fu, F., Crespy, D., Landfester, K. & Jiang, S. In situ characterization techniques of protein corona around nanomaterials. *Chemical Society Reviews* (2024).

38 Bilardo, R., Traldi, F., Vdovchenko, A. & Resmini, M. Influence of surface chemistry and morphology of nanoparticles on protein corona formation. *Wiley Interdiscip Rev Nanomed Nanobiotechnol* **14**, e1788, doi:10.1002/wnan.1788 (2022).

39 Sun, H., Jiang, C., Wu, L., Bai, X. & Zhai, S. Cytotoxicity-Related Bioeffects Induced by Nanoparticles: The Role of Surface Chemistry. *Front Bioeng Biotechnol* **7**, 414, doi:10.3389/fbioe.2019.00414 (2019).

40 García-Álvarez, R., Hadjidemetriou, M., Sánchez-Iglesias, A., Liz-Marzán, L. M. & Kostarelos, K. In vivo formation of protein corona on gold nanoparticles. The effect of their size and shape. *Nanoscale* **10**, 1256-1264 (2018).

41 Piella, J., Bastús, N. G. & Puntes, V. Size-Dependent Protein–Nanoparticle Interactions in Citrate-Stabilized Gold Nanoparticles: The Emergence of the Protein Corona. *Bioconjugate Chemistry* **28**, 88-97, doi:10.1021/acs.bioconjchem.6b00575 (2017).

Supplementary Files

This is a list of supplementary files associated with this preprint. Click to download.

- Supplementaryinformation.pdf